Available online at www.sciencedirect.com
SCIENCE DIRECT®
Coordination Chemistry Reviews 248 (2004) 1181–1194
COORDINATION CHEMISTRY REVIEWS
www.elsevier.com/locate/ccr

Review

Random walk models of charge transfer and transport in dye sensitized systems

Jenny Nelson*, Rosemary E. Chandler

Department of Physics, Imperial College London, Prince Consort Road, London SW72BW, UK

Received 30 December 2003; accepted 6 April 2004
Available online 28 May 2004

Contents

Abstract

Electron transport in porous, nanocrystalline metal oxide electrodes exhibits many features typical of dispersive transport in disordered semiconductors. This disorder can be attributed to energetic disorder in localized electron transport sites, or 'trap' sites. A numerical model based upon the continuous-time random walk (CTRW) is introduced to describe electron dynamics. The model is applied primarily to explain the stretched-exponential kinetic shape and strong bias dependence of optically observed recombination of electrons with photo-oxidized dye molecules, with the conclusion that recombination is limited by electron diffusion through a distribution of trap states. Analogous experimental and modelling studies of the functionally important back reaction between electrons in the metal oxide and oxidized species in the redox couple indicate that this recombination pathway is also dominated by trap-limited electron diffusion. The model predicts that such dispersive charge transport should be observed only on time scales shorter than the release time from the deepest trap, and this feature is used to explain the transition from fast, dispersive recombination kinetics slow and monoexponential behaviour in the presence of a slow (>10 ms) process limiting interfacial electron transfer. It is shown how transient optical measurements combined with modelling can be used as a probe of local electron dynamics, using inter-particle electron transport as an example. Finally, the application of random walk methods to simulation of device current–voltage characteristics is discussed.

Keywords: Dye-sensitized; Titanium dioxide; Solar cell; Dispersive transport; Modelling; Charge transport

1. Introduction

Dye-sensitized nanocrystalline metal oxide solar cells have become one of the most promising and intensively

* Corresponding author. Tel.: +44-20-7594-7581; fax: +44-20-7581-3817.
E-mail address: jenny.nelson@imperial.ac.uk (J. Nelson).

0010-8545/$ – see front matter © 2004 Elsevier B.V. All rights reserved.
doi:10.1016/j.ccr.2004.04.001

studied novel approaches to low-cost photovoltaic energy generation. Their design and function is well documented in other papers in this special issue and elsewhere [1,2]. The device is based upon a porous, nanocrystalline metal oxide electrode whose large surface area gives the device its high optical depth, and whose function is to conduct photoinjected electrons to an external circuit. Efficient device function requires that electron transport in this porous membrane be efficient relative to recombination. The physical description of electron transport is complicated, however, by the fact that the electrode is porous, granular and nanostructured. The consequence of porosity, when the electrode is permeated with a concentrated electrolyte, is that macroscopic electrostatic potential gradients cannot be supported and the bulk of the film is effectively field free [3,4]. Electron transport must therefore be dominated by diffusion. Any driving force for charge separation must be provided by the interfaces, and not by the macroscopic 'band bending' that is present in inorganic semiconductor devices. Granularity and porosity both mean that electron transport in the electrode may be strongly affected by interface and surface defects. The large surface area also presents a large area for electron recombination with the hole transporting medium in the pores. Porosity further suggests that charge transport may be influenced by geometry, through percolation effects. When compared with the crystalline, planar, field-bearing p–n junctions used in silicon solar cells, it is quite remarkable that the nanocrystalline electrode succeeds in transporting close to 100% of the photogenerated electrons to the external circuit without loss [5,2].

This paper is concerned with the mechanisms of charge transport and recombination in dye sensitized electrodes, and the search for a working model of the charge transport mechanism that is capable of relating the unusual material properties with experimental observation. A suitable model was found by adapting numerical models of 'dispersive transport', previously developed for amorphous semiconductors. The surprising result is the extensive influence of charge trapping on the kinetics of charge transfer, as well as charge transport. The model has provided a framework within which kinetics of different phenomena and their influence on device performance can be evaluated quantitatively. This paper focuses in on interpretation of measurements of interfacial charge transfer kinetics, which turns out to be strongly influenced by the mechanism of charge transport and is uniquely capable of probing electron dynamics on a local scale.

The paper is organized as follows. In Section 2 the concept of 'dispersive' charge transport is introduced and the experimental evidence for dispersive transport in nanocrystalline metal oxide electrodes is reviewed. In Section 3 the continuous-time random walk model for the dynamics of charge recombination between electrons and photo-oxidized dye molecules is described. The principal result is that electron trapping in the metal oxide is normally the process limiting the rate of electron–dye cation recombination, and that this behaviour is observed in a range of materials systems, although the specific parameters are a function of chemical materials. The model is validated by comparison with data for a range of material systems, and by comparison with other models. In Section 4 we show how, in the limit of slow interfacial charge transfer, the model predicts the appearance of slow, monoexponential kinetics resulting from competition between electron detrapping and the final, interfacial electron transfer step. In Section 5 we address the mechanism of the 'back reaction' between electron and redox couple, which is the predominant loss pathway affecting device function, and review a combined experimental and modelling study of the kinetics of this reaction which indicates that electron transport is again the rate determining step. In Section 6 we show how the electron–dye recombination reaction can be used to probe local electronic processes, and in particular we evaluate the influence of inter-particle electron transfer on electron transport using this approach. Section 7 addresses the application of random walk models of electron transport to simulation of photocurrent generation in devices.

2. Transport in dye-sensitized electrodes and 'dispersive transport'

2.1. Electron transport in nanocrystalline metal oxide electrodes

Electron transport in the porous nanocrystalline metal oxide electrode of a DSSC is both slow (of order of milliseconds for films of order 10 μm thick [6–10]) and very efficient at short circuit. Although electron transport is widely agreed to proceed by diffusion, the observed dynamics are not representative of simple diffusional processes, but contain evidence for charge trapping and trap filling. In particular photocurrent transients possess a slow tail typical of charge trapping [6–8] which in some conditions decays as a power law [9,10]; frequency resolved photocurrent measurements exhibit multiple time scales [11]; the effective diffusion constant appears to be electron density dependent [7,12,13]; photocurrent rise time is electron density dependent and shows a point of inflection typical of trap filling [14–16]. There is some evidence that that this behaviour is intrinsic to the nanocrystalline metal oxide films and is not solely a result of the interaction with the supporting electrolyte. For example, solid state nanocrystalline TiO_2-metal Schottky barrier structures show power-law photocurrent transients [17]; while strong evidence of charge trapping is seen in the transient photoconductivity of nanocrystalline TiO_2 films in gaseous ambients [16].

Additional evidence, of key importance to the work described here, comes from transient optical studies of the re-reduction of photo-oxidized dye molecules after excitation by a laser pulse. When the reaction is studied in a redox inactive electrolyte, the only species available to reduce the

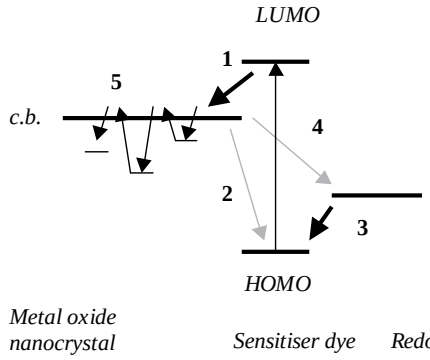

Fig. 1. Schematic of electron transfer steps in a DSSC. Photoexcitation of a surface attached dye molecule leads to rapid electron injection into the conduction band of the TiO_2 nanocrystal (1), while the dye is regenerated by electron transfer from a redox couple (3). Loss pathways are recombination of the electron with the dye cation (2) or directly with the redox couple (4). (4) is normally believed to be the predominant loss mechanism. Electron trapping in the nanocrystals (5) appears to limit the rate of electron transport and of recombination, via both pathways.

dye cation is the electron in the 'conduction band' of the TiO_2 (pathway 2 in Fig. 1). The transfer rate should thus depend on the availability of electrons near to the dye cation and the oxide–cation wave function overlap. This reaction was studied in detail by Haque et al. [18] using externally applied bias to modulate the background electron density in the TiO_2. The observed kinetics displayed a wide range of time scales and an unexpectedly strong dependence on applied bias, as shown in Fig. 2. The kinetic curves are best approximated by 'stretched-exponentials', $\Delta OD(t) \propto e^{-(t/\tau)^{\alpha}}$,

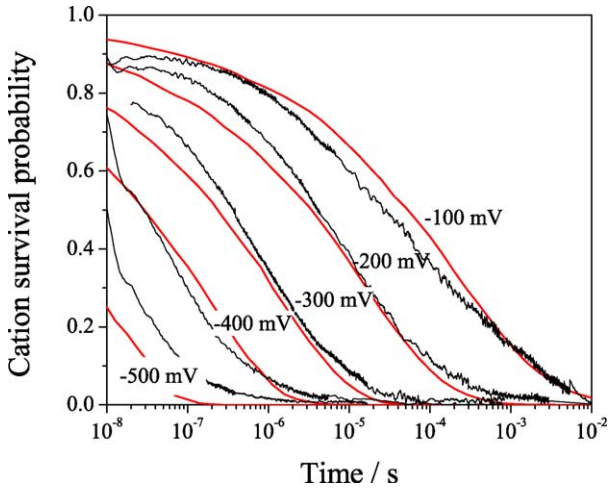

Fig. 2. Kinetic traces showing dye cation recombination with electrons in a dye-sensitized TiO_2 film after photo-excitation by a laser pulse, at several different applied biases in a redox inactive electrolyte, from Ref. [32]. The dye cation survival probability is obtained from the change in optical density of the dye cation normalized to the initial change after the laser pulse. Simulated results using the multiple trapping CTRW model are represented by smooth lines. Reprinted with permission from Ref. [32].

where $\Delta OD(t)$ represents the change in optical density due to oxidized dyes a time t after the laser pulse, and τ and α are constants. The bias dependence translates into a dependence on electron density, n, once the form of the electronic density of states (DoS) is known.

The observed behaviour could not be explained by either of two anticipated mechanisms: in the limit of fast interfacial electron transfer, recombination would be expected follow second order kinetics and the dye cation lifetime to vary like $1/n$, assuming that electrons follow normal diffusion; in the limit of slow interfacial electron transfer then the recombination rate should depend upon the electron–dye cation wave function overlap and be independent of n, although some dispersion in rates could be introduced by disorder in the interfacial free energy difference. Neither mechanism predicted the observed strong bias dependence. An explanation was found instead in the concept of dispersive electron transport.

2.2. Dispersive transport and the continuous-time random walk

The concept of 'dispersive transport' was introduced in the 1970s to describe charge transport phenomena in disordered semiconductors such as amorphous silicon and amorphous compound semiconductors [19–21]. The central idea is that charge carriers become trapped in localized, or 'trap' states so that the kinetics of charge transport are dominated by the time constants for release from those sites. In a disordered electronic material, these rates may be distributed as a result of energetic disorder (in the case of transport by thermal activation) or configurational disorder (in the case of variable range hopping). Transient phenomena observed on time scales shorter than the longest of these rates for the studied system are 'dispersive' and lead to poorly defined average physical properties, which may depend on the observation window. A common signature of dispersive transport is a transient photocurrent with asymptotic time dependence of the form $I(t) \propto t^{-1-\alpha}$, where α is a constant such that $0 < \alpha < 1$. A numerical model for such 'anomalous' diffusion, was proposed by Scher and Montroll [20] using a 'continuous-time' random walk (CTRW) where charge carriers move by diffusion on a lattice, but with a time step drawn from a waiting time distribution, $\psi(t)$. Scher and Montroll used a power-law waiting time distribution of the form

$$\psi(t) \propto t^{-1-\alpha}. \quad (1)$$

This contrasts with 'normal' diffusion where the time step should be drawn from a Poisson distribution, $\psi(t) \propto e^{-t/\tau}$, equivalent to a random walk with a mean step time τ. The CTRW model is easily implemented using Monte Carlo simulations on a lattice and the use of an adaptive time step allows systems with widely differing time scales to be simulated without excessive computational cost. Though applied by Scher and Montroll to measurements of

time-of-flight photocurrent transients, the CTRW has also been applied to the kinetics of scavenging [22] and annihilation [23] reactions in disordered media, and to exciton transport in light harvesting systems [24]. The annihilation reaction, $A + B \rightarrow 0$ is the analogue of diffusion limited bimolecular recombination but in a dispersive medium. For the case of annihilation of immobile species, or 'targets' (A), by encounters with an excess of mobile species, or 'walkers' (B), the target survival probability ϕ_A varies like

$$\phi_A(t) \propto \exp(-S(t)) \tag{2}$$

where $S(t)$ is a function representing the number of sites visited by walkers in time t [25]. For a normal random walk where $S(t) \propto t$ the kinetics take the usual quasi-first order form expected when $B \gg A$, i.e. $\phi_A(t) = \phi_0 e^{-t/\tau}$. For a continuous-time random walk characterized by the waiting time distribution (1), $S(t)$ has the asymptotic form $S(t) \propto t^{\alpha}$ [26] with the result that ϕ_A varies like a stretched-exponential

$$\phi_A(t) = \phi_0 e^{-(t/\tau)^{\alpha}} \tag{3}$$

In the limit where A and B are initially equal, each population decays like a power-law at long times, again characterized by the exponent α,

$$\phi_A(t) = t^{-\alpha} \tag{4}$$

Stretched-exponential kinetics are often observed for relaxation processes in disordered electronic and molecular systems [27–29]. Physically, a waiting time distribution of exactly the form (1) may arise from thermal activation out of an exponential distribution of trap states. A distribution similar to (1) may also arise from variable range hopping between localized sites with a uniform, random spatial distribution [19].

3. Continuous-time random walk model for charge recombination in dye sensitized electrodes

3.1. CTRW applied to electron–dye cation recombination

The CTRW is an attractive model for the electron–dye recombination kinetics in dye sensitized TiO_2 electrodes on account of the prediction of stretched-exponential kinetic behaviour and its relevance to disordered semiconductors. A microscopic mechanism based on thermal activation out of exponentially distributed electron traps seemed more plausible than hopping between spatially distributed 'trap' states, although both were tested [30]. In order to explain the experimental data the model had to be modified to allow trap filling at high electron densities. This was achieved by assigning energies to specific trap sites and imposing a rule forbidding multiple occupancy, rather than using the Scher–Montroll approach of a waiting time distribution corresponding to the distribution of site energies. The occupancy rule results in Fermi-Dirac statistics for the trap state occupancy [31].

In its simplest version, the CTRW is executed as follows: A simple cubic lattice is generated where the ith site has an energy E_i drawn from the distribution

$$g(E_i) = \frac{1}{kT_0} e^{-(E_c - E_i)/kT_0} \tag{5}$$

where T_0 is the characteristic temperature of the distribution, k Boltzmann's constant and E_c is the conduction band edge energy. For simulations described here the simulation space is typically a sphere of radius 15–20a, where a is the lattice constant (of ~0.4 nm for anatase TiO_2), representing a nanoparticle of about 15 nm diameter, though identical results (to within a time scale factor) are obtained for a cubic domain with periodic boundary conditions. Electrons may move in this lattice by performing a random walk where the waiting time for an electron in a site of energy E_i ($<E_c$) is given by

$$t_i = -\frac{\ln X}{\nu_0} e^{(E_c - E_i)/kT} \tag{6}$$

where ν_0 is the attempt-to-jump frequency and X is a random number between 0 and 1. The destination site is one of the unoccupied nearest neighbours and is chosen at random. To simulate equilibrium a density n_d of electrons, representing the background and electrically injected electron density, is located at random on the lattice and allowed to diffuse in this way. The dynamics are handled using a queue, where first the electron with the shortest waiting time is moved, and then the queue is resorted, and simulation and waiting times advanced, after each step. A laser pulse experiment is simulated by generating n_g additional electrons and n_g dye cations, or 'targets', at random locations at time $t = 0$. n_g is known from the optical absorbance and laser intensity, and uniform distribution is justified by the low optical densities used in transient optical experiments. The electrons are allowed to diffuse and when an electron walks on to a site occupied by a dye cation the pair recombine. Physically this 'reactive site' may represent the site on the metal oxide lattice that is closest to the adsorbed dye cation. The prompt recombination implies a much faster rate for electron transfer to the dye cation than to any neighbouring lattice site. The populations are then decremented and the dye cation lifetime recorded. The simulation continues until the dye cations are exhausted. The simulated dye cation survival probability $\phi(t)$ is built up from the distribution of dye cation lifetimes over many simulations, for given values of n_d, n_g and T_0.

The resulting survival probability varies as a stretched-exponential (3) where $\alpha = T/T_0$, and the characteristic time constant τ decreases with increasing n, where $n = n_d + n_g$. Experimental data are usually characterized by a half-life, $\tau_{50\%}$, which relates to τ through $\tau_{50\%} = \tau(\ln 2)^{1/\alpha}$. The exponent in Eq. (3) should vary in proportion to n since $S(t)$

represents the number of sites visited by walkers in time t. Hence $\tau_{50\%}$ should vary with n like

$$\tau_{50\%} \propto n^{-1/\alpha} \tag{7}$$

Thus the apparent order of reaction with respect to n is controlled by the exponent of the density of states function, and may be very large. Large orders (up to 4) are indeed observed [30,32].

An alternative view of the kinetics is that only a fraction, n_{free}, of the electron population is available to take part in recombination (or transport) at any time. (It is assumed that carriers which are trapped at sites not adjacent to the dye cation do not take part in recombination while trapped; this is supported by a comparison of models with and without long-range hopping to the dye cation in Ref. [30].) With Fermi-Dirac statistics it is easily shown that [13,31]

$$n_{\text{free}} \propto n^{1/\alpha} \tag{8}$$

Since for bimolecular recombination the lifetime of the target, (A), varies like the inverse of the density of walkers, (B), where walkers outnumber targets ($[B] \gg [A]$), we recover the same behaviour as Eq. (7):

$$\tau_{50\%} \propto \frac{1}{n_{\text{free}}} \propto n^{-1/\alpha}$$

Note that the above argument leads to an electron density dependence of the effective mobility $\mu(n)$: If the free electrons diffuse normally with a density independent mobility μ_{free} then the effective mobility $\mu(n)$ must satisfy [33,34]

$$\mu_{\text{free}} n_{\text{free}} = \mu(n) n \tag{9}$$

whence $\mu(n) \propto n^{(1-\alpha)/\alpha}$. Similar n dependences for the effective diffusion coefficient and recombination coefficients can be found.

The model as described above has been applied to simulate the recombination of electrons with dye cations in a range of chemical environments (TiO_2 in ethanol electrolyte without lithium [18,32], TiO_2 in dry acetonitrile with lithium ions (0.1 M $LiClO_4$) [30], ZnO in dry acetonitrile with and without lithium ions [35], TiO_2 in propylene carbonate with 0.1 M $LiClO_4$ [36]) and the behaviour of Eqs. (3) and (7) has been reproduced (Fig. 3). The similar qualitative behaviour of the different systems (summarized in Fig. 3(a)) supports the idea that electron–dye cation recombination kinetics are dominated by trap-limited electron diffusion in all these systems. The simple model is thus able to explain the transient shape and the strong bias dependence of the observed dye re-reduction kinetics, and also why the recombination is unexpectedly slow in unbiased systems.

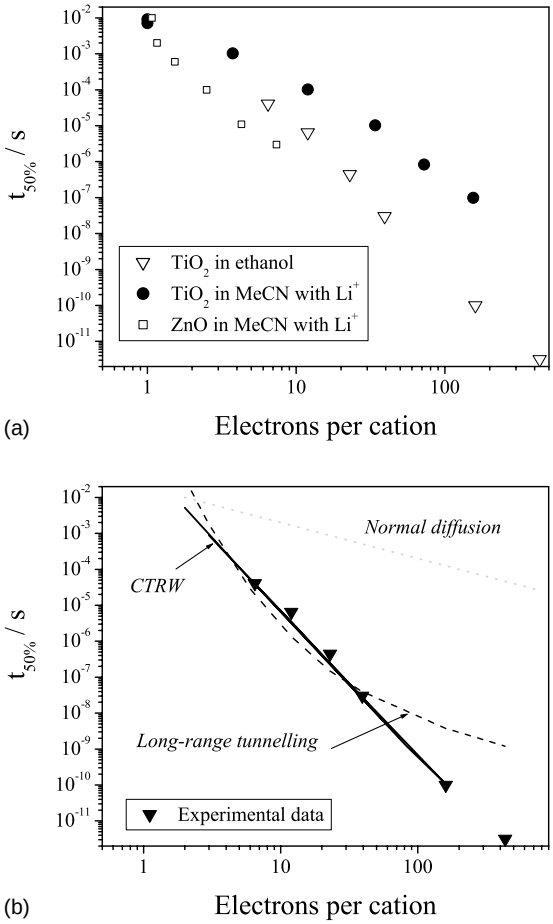

Fig. 3. (a) Dye cation half-life, $t_{50\%}$, as a function of the number of electrons per cation for three different metal oxide–electrolyte combinations. The different points in each set represent different applied biases. The $t_{50\%}$ value is obtained by transient optical spectroscopy (such as Fig. 2) and the electron densities are obtained from chronoamperometry or from infrared optical absorbance, or both (from Refs. [30,32,35]). (b) Dependence of dye cation half-life, $t_{50\%}$, on electron density as predicted by the multiple trapping CTRW model (full line), the long range tunnelling model (dashed line) and for recombination limited by simple, trap-free diffusion (dotted line) in comparison with experimental data for the TiO_2–ethanol electrolyte system [30]. Only the CTRW model reproduces the strong power-law behaviour shown by the data. Reprinted with permission from Ref. [30].

3.2. Justification of assumptions and evaluation of alternative models

Before extending the model to other situations we will attempt to justify the underlying assumptions and the meaning of parameters used. The model is based on the following assumptions:

(1) that recombination is limited by the time taken for arrival of an electron at a reactive site next to an adsorbed dye cation;
(2) that electron transport is dominated by the distribution of trap energies and not by the details of the microscopic (e.g. lattice) or macroscopic (grain size and intergrain) geometry, and that the chemical environment enters only through the parameters T_0, n_d and ν_0;
(3) that the dominant electron transport mechanism is thermal activation out of a localized site to a nearest neighbour via a 'conduction band', and is not influenced by

long range interactions. We will call this preferred mechanism 'multiple trapping'.

Question (1) is dealt with in Sections 4 and 5, where we show how in certain conditions the recombination kinetics become dominated by a slower, interfacial process and the kinetics become monoexponential. We stress here that the shape of the kinetic curves at a single bias is insufficient to determine a model. Several groups have shown that the multiphasic kinetics observed in transient optical experiments can be fitted to some combination of second order processes [37,38]. However, the second order models are incapable of explaining the very strong dependence of kinetics on applied bias.

Regarding question (2), the issue of intergrain versus intragrain transport is addressed in Section 6. The effect of geometry within a grain has been addressed in Ref. [30], where it is shown that for a sufficient density of deep traps the effect of imposing different geometries on the simulation space or on the location of traps is only to change the time scale through the factor ν_0, and does not change the temporal form of the kinetics or their n dependence. For most simulations we use a cubic lattice enclosed in a sphere or a spherical shell, as a crude model of a nanoparticle.

The proposed multiple trapping transport mechanism (question (3)) has a physical justification for electron transport in TiO_2. There is substantial evidence that the mechanism of electron conduction, at least in rutile TiO_2, is small-polaron hopping. Conduction electrons localize on sites occupied by transition metal ions (Ti^{4+}) and are bound there by a potential well due to the distortion of the surrounding lattice by the negative charge on the extra electron, i.e. the electron "digs its own potential well" and may be described as 'self-trapped' [39]. Conduction electrons thus create Ti^{3+} species. To move, the electron must overcome a potential barrier to hop to a neighbouring Ti^{4+} site, bringing its associated lattice distortion. In rutile the small polaron activation energy is reported to be a few tenths of an eV [39,40].

There is, moreover, significant evidence that the predominant defects in TiO_2, both anatase and rutile, are similar in nature to Ti^{3+} states. In particular, oxygen deficient rutile TiO_2 possesses electronic states with 3d electronic character located some few tenths of an electron-volt below the conduction band edge [41]. Electronic structure calculations confirm that oxygen deficiency should lead to Ti^{3+} defect states of 3d character [42]. Anatase crystals, though less well studied, reveal a similar oxygen dependent gap state some 1 eV below the conduction band edge when studied by photoelectron spectroscopy [43]. Application of a negative potential [44] and doping by intercalation of lithium ions [45] or surface binding of other metal cations [46] have been shown to lead to electron localisation on Ti^{3+} defect sites.

The high surface area and small particle size of nanocrystalline TiO_2 indicates that defects may be expected both at the surface and through the 'bulk' of the film, and the above evidence suggests that many of these will be some form of Ti^{3+} state, though the variations in origin and location may well lead to variations in the binding energy. The physical basis of our model is therefore that electrons move on the TiO_2 nanocrystal lattice by thermally activated small polaron hopping between neighbouring Ti sites, some of which may be stoichiometric 'self trapping' sites and some intrinsic or extrinsic defects, and that the energies of the sites are distributed on account of the variations in origin and nature.

A useful consequence of the nature of the conduction band electron states is the appearance of optical absorption in the red–infra-red when the material is doped with electrons [3,44,47]. This absorbance can be attributed to an optically allowed transition between the lowest lying 3d orbitals, of t_{2g} symmetry, of the Ti ion, and higher e_g orbitals, whose degeneracy is lifted by the octahedral crystal field of the surrounding oxygen ions [48]. (Such transitions are known to lead to a violet colour in hydrated TiO_2.) It may also be compared to free electron absorbance in semiconductors, though there is evidence that the absorbing electrons in nanocrystalline TiO_2 are not completely free but are trapped [48–50]. In Section 5 below we will describe how this optical signature of conduction band electrons in TiO_2 can be used to probe the dynamics of electron recombination with the redox couple in the electrolyte.

Alternative microscopic models of electron transport include variable range hopping and 'random flight'. A long range tunnelling model was evaluated in comparison with the multiple trapping transport mechanism in Ref. [30]. In the tunnelling model, trapped electrons experience long range interactions, by which they tunnel to other, vacant trap sites or to the dye cation, according to a Miller–Abrahams model for the thermally activated transition rate (Fig. 4). In this case recombination occurs after a short sequence of long hops. In Ref. [30] it was shown that while the multiple trapping model could explain both the observed kinetic curves and the dependence of $t_{50\%}$ on n, the tunnelling model could not predict sufficiently strong n dependence of kinetics over the full range of experimental data, even in the limit of very few traps and extremely long tunnelling distances of several nm. The tunnelling model was effectively ruled out by comparison with data for sub-nanosecond recombination (Fig. 3(b)).

Barzykin and Tachiya have proposed an alternative model based upon the 'random flight' of electrons across a TiO_2 nanoparticle [51]. Electrons are effectively delocalized across the nanoparticle and captured at random by trap states. The model is mathematically similar to the CTRW and predicts similar behaviour but with a different physical interpretation. One difficulty with the application of that model to TiO_2 is the evidence that electrons tend to move by small-polaron hopping in TiO_2 rather than by scattering between delocalized states within a conduction band; however, the agreement between the two models is instructive and random flight may be appropriate for less polar materials.

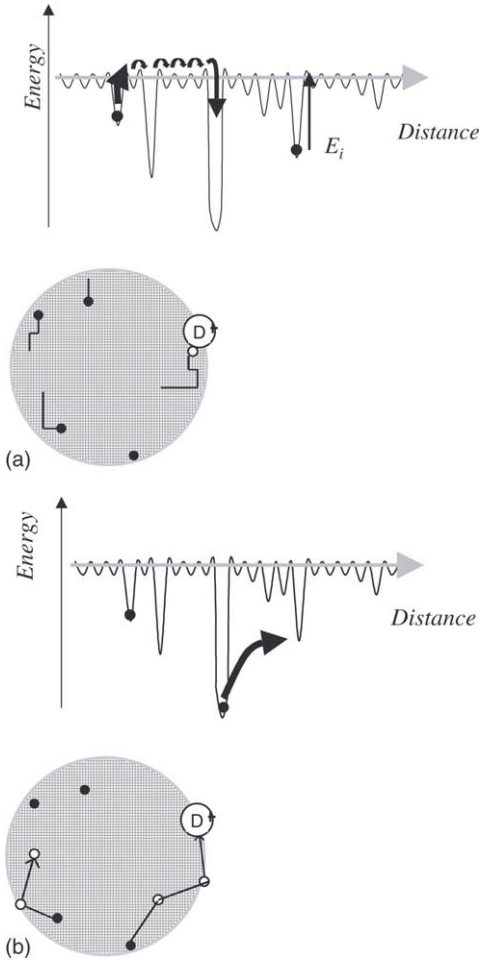

Fig. 4. Schematic of electron motion in (a) the multiple trapping CTRW and (b) the long range tunnelling models. Lower panels show a spatial schematic of electron transport inside a nanoparticle, represented by a regular cubic lattice embedded in a spherical space. Upper panels show transport as transfer between localized sites which are distributed in energy. In (a), electrons move at random between nearest neighbour sites with a waiting time which depends on the activation energy of the site currently occupied. Recombination occurs whenever an electron moves on to a reactive site occupied by the dye cation. In (b) electrons may tunnel over longer distances to other, vacant trap sites or directly to the dye cation. Only the multiple trapping random walk reproduces the observed dependence of dye cation half-life on electron density over the full range of time scales (see Fig. 3(b)).

3.3. Meaning of parameters

The kinetic curves are determined by the parameters T_0, n_d/n_g and ν_0. Physically, T_0 must represent the characteristic temperature of the DoS over the range of Fermi levels probed. There is no fundamental reason why electron traps in nanocrystalline TiO_2 and other oxides should adopt an exponential distribution. However, an approximately exponential dependence of electron density on applied bias in nanocrystalline metal oxide electrodes has often been observed [35,52] or inferred [9,10,13,53]. Note that experiment gives no information on the form of $g(E)$ outside the range of Fermi levels probed and so another form may apply at higher or lower energies. For example, a distribution approximately equal to an exponential over a limited range of energies is easily constructed from other forms such as the sum of two unequal Gaussians [31]. In this work we use the exponential DoS as a convenient empirical form. The characteristic temperature T_0 appears to be influenced by both electrolyte and metal oxide (values range from 600 to over 1000 K), though the relationship is not well defined.

The 'dark' electron density n_d has a clear interpretation. From a Fermi-Dirac perspective, n_d should vary like $n_d \propto \exp(E_F/kT_0)$, where E_F is the Fermi level of the metal oxide. In practice, shifts in E_F may not correspond exactly to $q\Delta V$, where ΔV is an externally applied bias step, indicating that part of the applied bias is dropped across the interfaces or lost to series resistance [30,32]. As the bias applied to the metal oxide is increased (more negative) n_d should increase relative to n_g resulting in two regimes: a low (or positive) bias regime where n is independent of n_d and kinetics are independent of bias, and a high (or negative) bias regime where $\tau_{50\%}$ decreases approximately like n^{-T/T_0} (Eq. (7)). Two such regimes have been observed in all systems studied, but with a threshold bias that depends on material. The threshold bias is more positive in those materials that have a higher electron density at equilibrium, due to either the higher background charge density (e.g. ZnO and SnO_2 compared to TiO_2 electrodes [35,54] or to the effect of potential determining Li^+ or H^+ ions [55].

n_d has a further effect, which is to determine the effective low energy cut-off for the density of states (equivalent to the electron Fermi level for equilibrium systems). This low energy cut-off determines the time scale at which transport becomes non-dispersive. This is discussed below in Sections 4 and 5. Increasing the background electron density, for instance by measuring recombination kinetics under steady state illumination, has the effect of cutting off the slow tail of the kinetic curve, in agreement with the model predictions [56,57].

The parameter ν_0 formally represents the attempt-to-jump frequency for a DoS of the form Eq. (5) that is a continuous exponential up to E_c, where all site energies are drawn from (5) and the probability P_{et} of electron–dye cation recombination upon meeting is unity. However, the value of ν_0 may differ from the actual attempt-to-jump frequency if the form of $g(E)$ above the highest Fermi level probed is not exponential, or if not all sites are 'traps', or P_{et} is less than 1. Therefore the correct physical interpretation of ν_0, is not well defined and ν_0 is best treated as a fitting parameter.

4. Limit of slow interfacial electron transfer

The model described in Section 3 supposes that kinetics are controlled by the intersite hopping rate ν_0 and the density of trap states. The interfacial electron transfer rate, k_{et}, is assumed so fast that electron–dye cation recombi-

nation occurs promptly upon meeting. Within the model it is clear that reducing ν_0 for any given DoS merely translates the kinetic curves to longer time scales. Such effects are indeed observed where faster or slower recombination in the low (or positive) bias regime is achieved by changing solvent or metal oxide. Such variations may be attributed to different mobilities in the oxide, or to the effect of solvent on charge transport, e.g. through ambipolar diffusion [33,58].

Introducing k_{et} as an explicit parameter leads to qualitative changes in the shape of the kinetic curves. When k_{et} is slow, release from trap states competes with the interfacial transfer step and the electron makes multiple encounters with the reactive site before a recombination event takes place. If the DoS is exponential down to deep energies, the effect is simply to slow down the kinetics by a constant factor, exactly like reducing ν_0. However, background electron density in the n-type oxide material introduces a low-energy cutoff to the effective DoS, and if the interfacial electron transfer time is comparable with the release time from these deepest states then the kinetic curves begin to change shape and become less dispersive. Recombination is no longer limited by the first passage time of an electron to a reactive site. In the limit where $1/k_{et}$ exceeds the time for release from the deepest effective trap, the kinetics become monoexponential, provided that k_{et} is similar for all dye cations in the system. This behaviour was observed by Clifford et al. [59] in a comparison of electron–dye cation recombination kinetics using a porphyrin dye and using a modified porphyrin dye in which triphenylamine side groups serve to locate the positive charge further from the TiO_2 surface. The modified dye led to slower, monoexponential kinetics (see Fig. 6 of paper by Durrant et al. in this issue). A continuous trend from fast, stretched-exponential kinetics to slow, monoexponential kinetics was observed using a series of different dyes in which the positive charge density of the cation is located, according to quantum-chemical calculations, at different distances from the carboxylate binding ligands [60]. Reducing k_{et} using barrier layers of a second metal oxide with smaller electron affinity also reduces both the rate of recombination and the dispersiveness of the kinetic curve [61]. From comparison of the time scales for fast, electron transport limited recombination and slow, interfacial transfer limited recombination we obtain an upper limit, of order 10 ms, to the time for electron release from the deepest trap state.

This competition between detrapping and interfacial electron transfer is readily incorporated into the CTRW model. In the simple model described above the probability of a recombination event when electron meets dye cation is one. To allow for variation in the rate of electron transfer to the dye cation, we introduce a fractional probability, P_{et}, for recombination once an electron reaches a reactive site. This represents a first order recombination process of rate $k_{et} = \nu_0 P_{et}$ which competes with electron release from the site

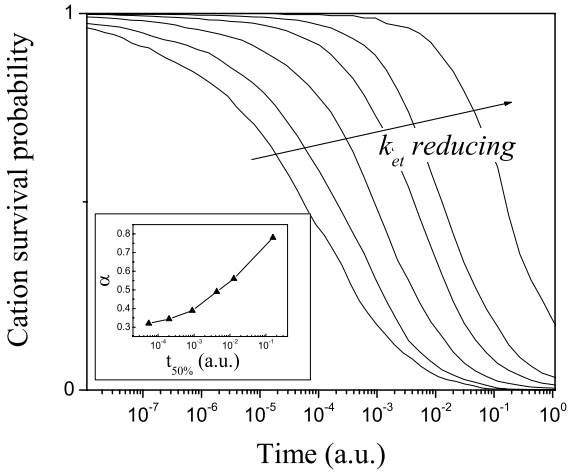

Fig. 5. Simulated kinetic curves for dye cation survival probability in a system with a fractional probability of electron–dye cation recombination upon meeting. The CTRW model is used with an exponential density of states with $\alpha = 0.3$. From left to right, the kinetic curves represent k_{et} values of 1, 0.3, 0.1, 0.03, 0.01 and 0.001 times the attempt to jump frequency (see text for explanation). As k_{et} is reduced, the apparent density-of-states parameter α, obtained by forcing a stretched-exponential fit to the kinetic curve, increases towards 1 as shown in the inset. Adapted from Ref. [75].

at a rate ν_0. If recombination does not occur, the electron continues its random walk and the simulation continues. In the limit where $P_{et} \to 0$, the recombination becomes reaction limited and the recombination rate tends to P_{et}/τ_{max}, where τ_{max} is the average time to visit all sites on the system, and is a function of the system size and the depth of the density of states. In this limit the kinetics are monoexponential.

The effect of k_{et}, on recombination dynamics was simulated using the CTRW model modified as explained above. The model system was similar to that used in Ref. [30] consisting of a spherical shell of radius 17 and thickness three lattice units, representing a TiO_2 nanoparticle with surface distributed traps. The room-temperature dispersion parameter α was 0.3 ($T_0 = 1000$ K) and simulations were carried out with one dye cation and three electrons, allowing for dark conduction electrons in the film (although the value of n_d does not affect results qualitatively). P_{et} was varied between 1, representing prompt recombination, and 0.001. Simulated kinetic curves are presented in Fig. 5. It is clear that the curve evolves from a stretched-exponential of dispersion parameter $\alpha = 0.3$ towards more monoexponential behaviour as P_{et} is reduced. The inset shows how the value of α extracted by forcing a stretched-exponential fit to the kinetic curves increases with decreasing k_{et}. In the limit of high k_{et}, the recombination dynamics are limited by the first passage time to the reactive sites, resulting in dispersive recombination dynamics as we have reported previously. In the limit of slow k_{et}, electrons must visit the reactive site many times before recombination occurs, resulting in a more monoexponential decay. Note that the value of k_{et} at which the

process becomes monoexponential reflects the time needed for the electron to freely explore the surrounding volume, and depends upon the effective electron mobility as well as the distribution of trap energies. The simulation results presented in Fig. 5 are in good agreement with the experimental results reported in Ref. [59,60].

5. Influence of charge trapping on the back reaction

The work described in Section 3 is concerned with reaction pathway 2, which has been shown [36,62] to be the less important of the two electron loss pathways in Fig. 1, at least in liquid electrolyte devices. Given the conclusion above that electron transport dynamics normally dominate the kinetics of pathway 2 it is of interest to know if they also control the kinetics of pathway 4. This question is relevant to device design and choice of materials: evidence from intensity modulated photovoltage spectroscopy studies indicates that the rate of electron recombination with the I_2/I^- electrolyte varies approximately like n^2, leading to long open-circuit electron lifetimes in solar cells at low light levels [63]. If electron dynamics follow normal diffusion this behaviour can be attributed to a reaction scheme for the reduction of I_2 that is second order in electron density [53]. However, as pointed out in Ref. [30], a superlinear dependence of recombination rate on n is also expected for trap-limited electron transport, according to Eq. (7) and the discussion above, even if the redox reaction is first order in n.

The question has been addressed experimentally in a recent transient optical study [64,65], analogous to those described in Section 3. Electrons are introduced by band gap excitation of a dye-free TiO_2 electrode and their density monitored by probing the change in absorbance at 800 nm where the absorption due to conduction electrons in nanocrystalline TiO_2 is strong. Transient optical spectroscopy of conduction electrons has been used previously in the frequency domain to study electron dynamics at short circuit and open circuit [62,66]. In the present work, electron–hole recombination is prevented by adding a hole scavenger such as methanol. (Methanol is well known to act as a hole scavenger [67] and has been shown to greatly enhance the lifetime of photoexcited electrons in nanocrystalline TiO_2 [16,64]. Comparison with different hole scavengers confirmed that the choice of hole scavenger had no observable effect on kinetics.) In a redox inactive electrolyte the absorbance signal due to the optically introduced electrons then lasts for hundreds of ms. When the I_2/I^- couple is introduced the electron absorbance decays on a time scale of ms, through recombination of electrons with the oxidized species in the redox couple. We will refer to this as the 'back reaction'. As the concentration of I_2 is increased from 1 to 100 mM, in an excess of I^-, the kinetics accelerate and change shape. At high $[I_2]$ where the concentration of I_3^- species available for reduction exceeds the photo-injected electrons, the signal is fast and stretched-exponential. (Given that the iodine exists predominantly as tri-iodide in the iodide rich electrolyte, we will refer here to the reacting species as I_3^-, though it is understood that the I_3^- dissociates into I_2 and I^- before the I_2 is reduced [10,53].) This is compatible with a recombination process which is rate limited by the diffusion of electrons through an energetically disordered landscape towards I_3^- 'targets' located on or near the surface of the nanocrystalline film. At low $[I_2]$ the kinetics become slow and monoexponential, apparently limited by the diffusion of I_3^- species from the bulk of the electrolyte towards the TiO_2 nanoparticle surface. In this limit the final, interfacial charge transfer step becomes limiting, exactly as in the case of slow electron transfer to the dye cation discussed in Section 4. The two regimes are illustrated in Fig. 6(a).

The process can be simulated with the CTRW, treating the electrons as 'walkers' and the I_3^- species as 'targets'. First order recombination with respect to electron density is simulated by allowing a recombination event as soon as an electron walks on to a site occupied by a target, in analogy with the electron–dye cation recombination model. A second order process is simulated by allowing the electrons to remain for a certain residence time with the target. If a second electron arrives at this pair before the first electron leaves then recombination occurs and all three species are removed from the lattice. For short residence times the intermediate electron–target complex is in equilibrium with its separate components and second order kinetics result. This is readily demonstrated by using a trap free lattice, where short residence times lead to an electron density that decays like $1/t$ at long times in an excess of targets, as expected from second order kinetics. Long residence times lead to quasi-first order behaviour.

In order to avoid including a full microscopic simulation of I_3^- diffusion in the electrolyte we make two approximations. We consider that only a fraction, F, of the electrolyte volume is available for recombination. This may be considered as the volume of a thin layer at the surface of the TiO_2 nanoparticle where the redox species are close enough to react with electrons in the nanoparticle. We treat F as a fitting parameter. As targets are removed from this layer by recombination they must be replenished (by diffusion) from the bulk of the electrolyte. The flux of targets from electrolyte into surface layer is simulated by analogy with a diffusive flux where new targets are introduced into the surface layer at a rate

$$J_I = k_D(I_{in} - I) \tag{10}$$

where I_{in} is the initial density of targets (equal to concentration of I_2) and k_D is an effective diffusion rate. The value of k_D is determined by the kinetic curves for low $[I_2]$, much as the kinetic curves for slow electron–dye cation recombination indicate k_{et}.

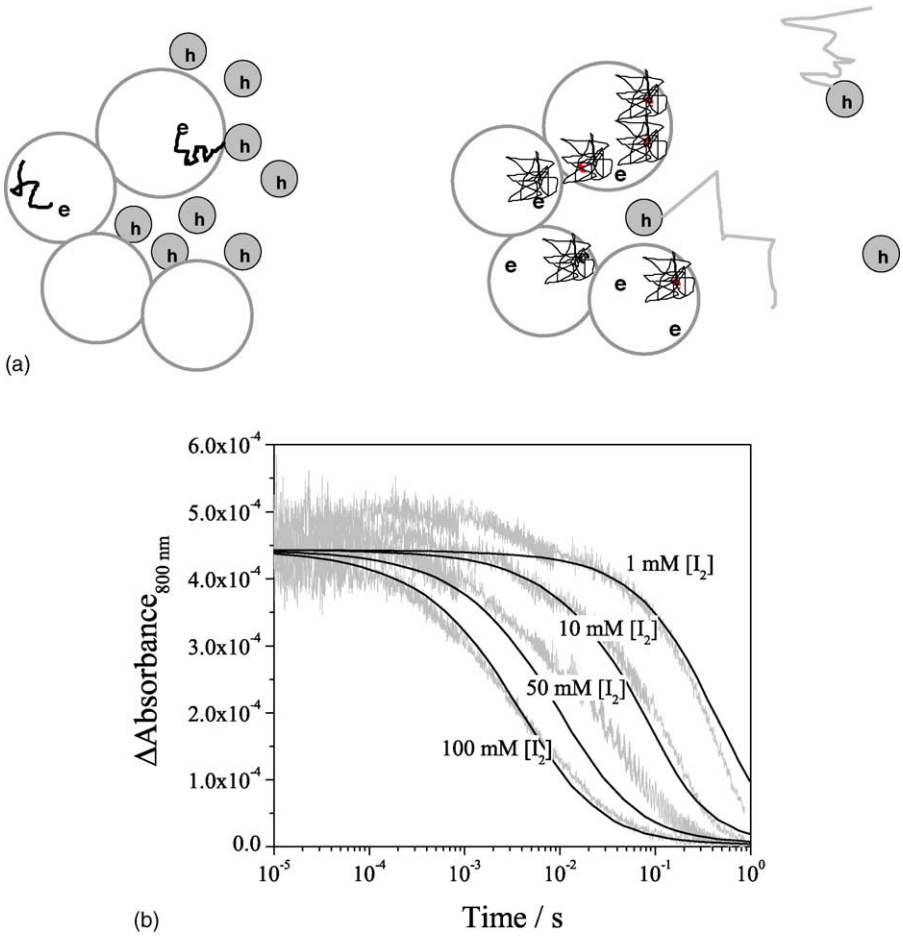

Fig. 6. (a) Schematic showing the two regimes for the electron–redox couple back reaction. Left panel: when the concentration of oxidized species, or 'holes' in the electrolyte (marked by 'h') is high recombination is limited by the diffusion of electrons towards the surface and kinetics are dominated by the dispersive electron detrapping process. Right: when the hole concentration is low, kinetics are limited by ion diffusion in the electrolyte. (b) Measured (grey lines) and modelled (black lines) change in absorbance at 800 nm, attributed to photoexcited electrons, in a dye free TiO_2 electrode in an electrolyte containing 0.6 M tetrabutyl ammonium iodide, 0.1 M lithium iodide and different concentrations of iodine in an acetonitrile solvent with 10% methanol to act as a hole scavenger. In the limit if high $[I_2]$ stretched-exponential kinetics are observed, similar to those for electron–dye cation recombination (Fig. 2). In the limit of low $[I_2]$ the kinetics become monoexponential [65].

Fig. 6(b) shows measured and modelled data for a set of samples with different I_2 concentrations using a first-order recombination model taken from Ref. [65]. The best fit to the data was achieved with $F = 0.05$ and $k_D = 4.5 \times 10^3\,s^{-1}$ although other combinations of these parameters gave reasonable fits. The first conclusion is therefore that the observed kinetics are consistent with a back-reaction that is first order in n. The second conclusion, apparent from the data alone, is that the order of reaction with respect to $[I_2]$ is first order as concluded by Liu et al. [63,68,69] and not second order as suggested by others [63,69].

Repeating the simulations with the second-order model leads to much poorer fits of the kinetics curves, for any set of parameter values, and to poorer fits of the dependence of the half-life on $[I_2]$ [65]. However, to confidently rule out a second order mechanism recombination should also be studied as a function of n.

If the kinetics of the back reaction are indeed first order in electron density, as this study suggests, then the observed superlinear n dependence of the recombination rate at moderate to high $[I_2]$ levels can be attributed solely to electron trapping in the TiO_2 and not to the details of the back reaction scheme. A similar conclusion was reached recently by Kopidakis et al. [10] from a study of the correlations between the rate of electron transport and the rate of back reaction in nanocrystalline TiO_2 electrodes in different chemical environments.

6. Dye as a spy: intra grain versus intergrain electron transport

The correlation of recombination kinetics with electron density provides a diagnostic tool for the physics of these systems. If kinetics are so strongly dependent on the elec-

tron density, we may use the kinetics as a probe of electron density in different configurations: this approach was used previously to show that the electron distribution through the films is approximately uniform [70]. In this section we show how optical measurements of recombination kinetics can be used to probe local electron dynamics, in order to evaluate the ease of inter-particulate, relative to intra-particulate, electron transport in a nanocrystalline film.

It has been proposed that the trapping of electrons within nanoparticles by inter-particulate barriers, leading to circuitous routes for charge collection, may be one reason for the very slow observed photocurrent transients [71–73]. Our study is based on the argument that the kinetics of recombination reflect the total number of electrons initially available to each dye cation. Thus, two dye cations and two electrons confined to a certain volume recombine, on average, faster than one dye cation with one electron confined to the half the volume of material. If electrons are confined within nanoparticles on the time scale of the measurement, then at low intensities where less than one dye is excited per nanoparticle, the kinetics should become intensity independent, as there is always only one electron initially available to the dye cation within the nanoparticle volume. If, on the other hand, electrons are free to move between neighbouring particles, then recombination kinetics will continue to slow down as light intensity is reduced even at low illumination levels. The two situations are illustrated in Fig. 7(a).

To address this question, we have extended the continuous-time random walk model discussed above to a multi-particle geometry. We incorporate the effect of restrictions between particles by considering a string of spherical particles connected by necks of area x times the geometric cross sectional area of a particle. Physically, x may represent a small contact area, a barrier for interparticle transport, or a high scattering probability at the grain boundary. We have simulated the kinetics of electron–dye cation recombination for photogenerated electron–cation pair densities, n_g, from 0.1 to 3 per nanoparticle for a trap distribution with $T_0 = 750\,\mathrm{K}$ ($\alpha = 0.4$ at room temperature) and different values of x. The simulated $\tau_{50\%}$ values, with an arbitrary time scale factor, are plotted against n in Fig. 7(b). For poorly connected nanoparticles (x values approaching zero), the kinetics clearly saturate when $n < 1$. For well connected particles, the kinetics continue to slow down monotonically as electrons explore a larger and larger volume to find the dye cation.

The model can be compared with experimental measurements of electron–dye cation recombination kinetics as a function of light intensity in redox inactive environments [55,74]. Those measurements were done without applied bias to maximize the effect of light intensity (i.e. to maximize n_g relative to n_d, so that $n_g \approx n$). Data for $\tau_{50\%}$ as a function of n, from Ref. [74] are plotted in Fig 7(b) in comparison with the simulation. (The time scale of the simulation is arbitrary.) It is clear that the experimental kinetics are intensity dependent down to low illumination levels with virtually no change in the dependence of $\tau_{50\%}$ on n.

This shows that interparticle transport is facile on the time scale of the measurement (100 μs–10 ms). The result indicates inter-particle trapping is not solely responsible for the slow electron transport, and supports the proposal that intraparticle trapping is sufficient to cause the observed dispersive behaviour. However, some influence of inter-particle retardation cannot be ruled out on the basis of these data alone; studies of different film morphologies would help to clarify the situation. A preliminary comparison of sintered and unsintered films suggests that interparticle transport may be slowed down, and $\tau_{50\%}$ beginning to saturate, in the unsintered film [74].

The conclusion agrees with recent experimental studies by Benkstein et al. [73] who find that geometric effects influence transport only weakly for porosities less than 60%, which are typical for working electrodes in dye sensitized solar cells. Further evidence that interparticulate transport is facile in nanocrystalline electrodes used in devices is given by the very high photocurrent quantum efficiencies available at short circuit is good working devices [5]. These show that even if inter-particle transport is restricted, it does not seem to result in completely inaccessible regions of film.

7. Charge transport in devices: applications and implications

Until now we have dealt with simulation of transient optical experiments. These effectively probe electron transport in a local scale, of the order of a few nanoparticles and so are well suited to microscopic Monte Carlo simulation with hopping distances of a few Angstroms. Monte Carlo random walk models are impractical, however, for microscopic simulation of photocurrent generation in complete devices, which are typically ∼10 μm and hundreds of nanoparticles thick. Yet it is clearly of interest to transfer models and parameters used to simulate transient optical phenomena to charge transport in operating devices.

One approach is to ‘renormalize’ the system and consider transport through larger units using hopping rules derived from the study of transport within those units. Provided that inter-grain effects are not dominant, and the background charge density is low enough for the trap distribution to be effectively exponential, then a useful approximation to larger scale transport can be achieved by renormalization of the waiting time distribution. Given a power-law waiting time distribution $\psi(t)$ of the form Eq. (1) for diffusion between units on a cubic lattice, a waiting time distribution $\psi_n(t)$ can be constructed for diffusion between cubic blocks of side n. Considering the Laplace transforms of $\psi(t)$ and $\psi_n(t)$ leads to a form for $\psi_n(t)$ which also varies like $\psi_n(t) \propto t^{-1-\alpha}$ in the limit of long times, though this result is only applicable to experiments on a time scale shorter than the longest detrapping time. Such a renormalized waiting time distribution was used in Ref. [32] to simulate power-law photocurrent

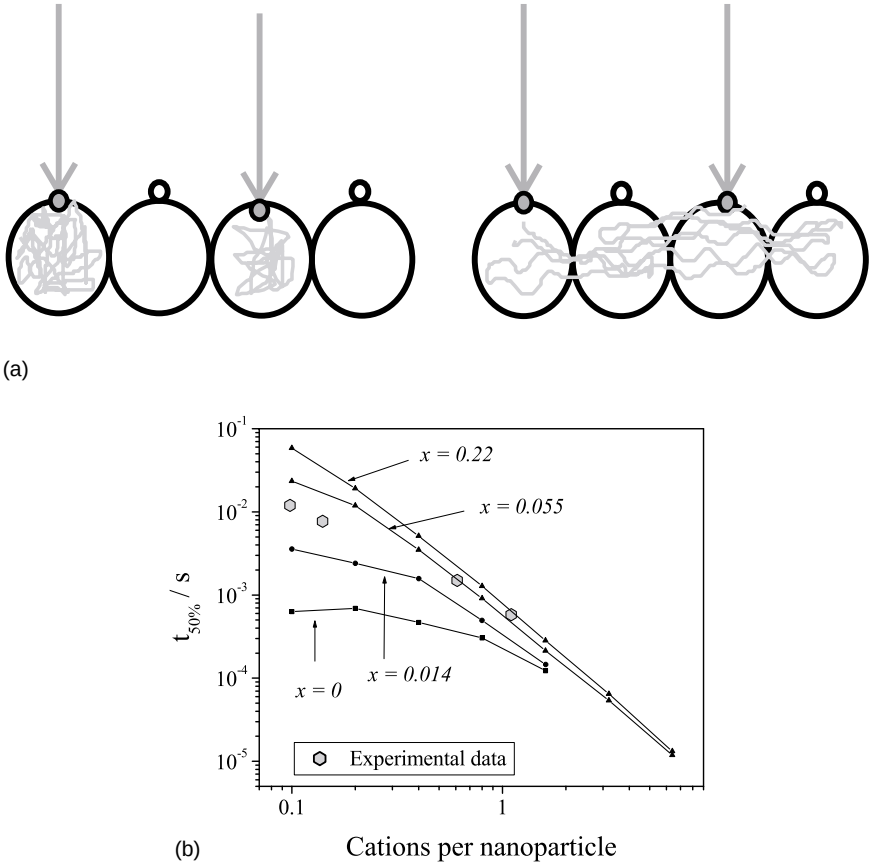

Fig. 7. (a) Schematic showing two different limits for the electron–dye cation recombination mechanism as the number of electron–cation pairs per nanoparticle falls below one. In the limit of no inter-particle transport (left) the photogenerated electron and dye cation are confined to a single nanoparticle and kinetics should become independent of the number of such pairs. In the limit of facile inter-particle communication (right) photoinjected electrons are free to explore the network of particles and recombination times continue to increase as the excitation density is reduced. (b) Simulated dye cation half-life in a connected chain of ten spherical nanoparticles, as a function of the number of cation–electron pairs excited per nanoparticle. Different curves show the effect of changing the cross sectional area of the neck between neighbouring particles, x (as a fraction of the maximum nanoparticle cross-sectional area). For very small neck area, kinetics saturate as intensity reduces towards 0; otherwise the dye lifetime increases continuously. Also shown are $t_{50\%}$ data taken from Ref. [74] for dye cation–electron recombination in a dye sensitized TiO_2 electrolyte in a redox inactive propylene carbonate electrolyte. The experimental data show continuous slowing as light intensity is reduced, consistent with facile inter-particle electron transport.

transients and demonstrate the effect of trap filling on transient decay and rise profiles. A similar approach was used by Van de Lagemaat and Frank to simulate photocurrent transients in Ref. [9]. By modulating the electron quasi-Fermi level to allow for trap filling, they were able to predict an observed transition from dispersive, power-law photocurrent transients over short collection distances to non-dispersive, exponential transients over longer collection distances and longer times (>10 ms). This transition is qualitatively similar to that observed for transport-limited and interface-limited recombination in Section 4, and results from similar physics.

A natural unit for a renormalized transport model is the component nanoparticle. In the limit of highly porous films where interparticle transport is limiting this unit would be physically sensible, and a useful model can be constructed by simulating a random walk between neighbouring nanoparticles in a simulated film. Benkstein et al. [73] use this approach to study the effects of geometry and morphology in films of different porosity and find that morphological effects dominate at porosities above 60%. A more detailed approach was taken by Cass et al. [72], who use a ‘fine scale’ Monte Carlo simulation to simulate electron transport over the range of a few nanoparticles, and compile a database of statistically similar trajectories, which are used as input into a larger scale simulation. That work clearly shows how the effect of traps can be accentuated by restricted inter-grain transport.

As a more practical alternative to Monte Carlo simulation of transport in devices, the microscopic transport model can be applied to find closed form approximations to the recombination coefficient and charge mobility. It is shown above that, for an exponential density of states, the density of free electrons with energy above some demarcation level or conduction band edge is related to the total electron density by Eq. (8), $n_{\text{free}} \propto n^{1/\alpha}$. This is consistent with the observed increase in recombination rate and in effective diffusion coefficient with increasing electron density. Eq. (8) can be used to define n dependent recombination and diffusion

coefficients in the continuity and current equations for electrons in a device, in a similar manner to Eq. (9). In a field free medium in one dimension, the continuity equation for electrons

$$\frac{\mathrm{d}}{\mathrm{d}x}\left(D\frac{\mathrm{d}n}{\mathrm{d}x}\right) + G - R = 0$$

becomes

$$D_0\frac{\mathrm{d}}{\mathrm{d}x}\left(\left(\frac{n}{n_0}\right)^{1/\alpha}\frac{\mathrm{d}n}{\mathrm{d}x}\right) + G - B_0 p n_0\left(\frac{n}{n_0}\right)^{1/\alpha} = 0 \quad (11)$$

where n_0 is some reference electron density at which D_0 and B_0 are defined. It is assumed here that the recombination is bimolecular for free carriers and that the density of positive charges is equal to n (no dark electrons). For a density of electron states other than purely exponential an empirical relationship between n_{free} and n can be found by Monte Carlo simulations of the steady state and used in Eq. (11). Eq. (11) can then be solved numerically together with corresponding continuity relation for the positive charge carriers and Poisson's equation. This was done in Ref. [57] to calculate the short circuit current density in polymer-fullerene solar cells, where hole polaron trapping appears to dominate the kinetics. Similar methods could be applied to model the current–voltage characteristics of dye sensitized solar cells, preferably after validation of the empirical forms for the recombination and diffusion coefficients against experimental data.

8. Conclusions

Many of the dynamic features of electrons in dye-sensitized electrodes are typical of 'dispersive transport', where kinetic dispersion is introduced through disorder in the energies of localized electron transport states. Here we have shown how a numerical model, the continuous-time random walk, which was introduced previously to describe charge transport in disordered amorphous semiconductors, can be adapted to describe the dynamics of electrons in dye sensitized electrodes. The kinetic behaviour of current and recombination transients can be directly related to the distribution of trap energies, which is typically exponential. The model is particularly suitable for simulation of transient optical studies of recombination, where the range of charge transport is limited to a few nanoparticles and a fully microscopic simulation of the dynamics is possible. Application of the model to a wide range of studies of the recombination reaction between electrons and dye cations in dye sensitized electrodes has shown that this reaction is normally rate limited by the diffusion of electrons through an exponential distribution of trap states in the metal oxide nanoparticle, and that this trap-limited diffusion is responsible for the high apparent order of the recombination with respect to electron density. Analogous studies of the kinetics of the functionally more important 'back reaction' between electrons in the metal oxide and the redox couple again indicate that the dispersive kinetics and high reaction order can be accounted for by electron trapping, rather than by a recombination reaction that is second order in electron density.

Dispersive electron transport is only observed on time scales shorter than the release time from the deepest trap, and when interfacial electron transfer is slowed down by reducing the interaction with dye cations or by reducing the availability of redox species, then a transition to mono-exponential, interface transfer limited kinetics is observed. Nondispersive behaviour is observed on time scales longer than order 10 ms.

Our studies of charge recombination indicate that the detailed effect of electron trapping on both transport and recombination must be incorporated into any useful numerical model of current–voltage characteristics of dye-sensitized solar cells. Although Monte Carlo simulation of a full device is not feasible, random walk simulations can be used to determine appropriate empirical forms for the electron density dependent diffusion and recombination coefficients, which can then be used in solution of the photocurrent–photovoltage equations.

Finally, we have shown how the sensitivity of recombination kinetics to electron density can also be used as a probe of local electron dynamics, and have used it to study the importance of inter-particle transport in nanocrystalline films. Our studies suggest that intra-particulate trapping is sufficient to explain the observed transport behaviour of sintered TiO_2 films.

Acknowledgements

The authors are grateful to Saif Haque, Emilio Palomares, Alex Green and James Durrant for useful discussions. We are grateful to Marc Jacouris and Saif Haque for permission to reproduce the experimental data presented in Fig. 7. We acknowledge the Engineering and Physical Sciences Research Council for financial support.

References

[1] A. Hagfeldt, M. Gratzel, Chem. Rev. 95 (1995) 49.
[2] M. Gratzel, Nature 414 (2001) 338.
[3] G. Rothenberger, D. Fitzmaurice, M. Gratzel, J. Phys. Chem. 96 (1992) 5983.
[4] J. Bisquert, G. Garcia-Belmonte, F. Fabregat-Santiago, J. Solid State Electrochem. 3 (1999) 337.
[5] M.K. Nazeeruddin, A. Kay, I. Rodicio, R. Humphrybaker, E. Muller, P. Liska, N. Vlachopoulos, M. Gratzel, J. Am. Chem. Soc. 115 (1993) 6382.
[6] A. Solbrand, H. Lindstrom, H. Rensmo, A. Hagfeldt, S.E. Lindquist, S. Sodergren, J. Phys. Chem. B 101 (1997) 2514.
[7] S. Nakade, S. Kambe, T. Kitamura, Y. Wada, S. Yanagida, J. Phys. Chem. B 105 (2001) 9150.

[8] N.W. Duffy, L.M. Peter, K.G.U. Wijayantha, Electrochem. Commun. 2 (2000) 262.
[9] J. van de Lagemaat, A.J. Frank, J. Phys. Chem. B 105 (2001) 11194.
[10] N. Kopidakis, K.D. Benkstein, J. van de Lagemaat, A.J. Frank, J. Phys. Chem. B 107 (2003) 11307.
[11] P.E. deJongh, D. Vanmaekelbergh, Phys. Rev. Lett. 77 (1996) 3427.
[12] L.M. Peter, K.G.U. Wijayantha, Electrochem. Commun. 1 (1999) 576.
[13] J. van de Lagemaat, A.J. Frank, J. Phys. Chem. B 104 (2000) 4292.
[14] K. Schwarzburg, F. Willig, Appl. Phys. Lett. 58 (1991) 2520.
[15] F. Cao, G. Oskam, G.J. Meyer, P.C. Searson, J. Phys. Chem. 100 (1996) 17021.
[16] J. Nelson, A.M. Eppler, I.M. Ballard, J. Photochem. Photobiol. A-Chem. 148 (2002) 25.
[17] R. Konenkamp, R. Henninger, P. Hoyer, J. Phys. Chem. 97 (1993) 7328.
[18] S.A. Haque, Y. Tachibana, D.R. Klug, J.R. Durrant, J. Phys. Chem. B 102 (1998) 1745.
[19] H. Scher, M.F. Shlesinger, J.T. Bendler, Phys. Today 44 (1991) 26.
[20] H. Scher, E. Montroll, Phys. Rev. B 12 (1975) 2455.
[21] R. Zallen, The Physics of Amorphous Solids, Wiley, New York, 1983.
[22] G. Zumofen, A. Blumen, Chem. Phys. Lett. 88 (1982) 63.
[23] A. Blumen, G. Zumofen, J. Klafter, Phys. Rev. B 30 (1984) 5379.
[24] E. Montroll, J. Math. Phys. 10 (1969) 753.
[25] A. Blumen, G.H. Kohler, in: M. Fleischmann, D.J. Tildesley, R.C. Ball (Eds.), Reactions in and on Fractal Media, in Fractals in the Natural Sciences, Princeton University Press, Princeton, 1990.
[26] A. Blumen, J. Klafter, G. Zumofen, in: I. Zschokke (Ed.), Optical Spectroscopy of Glasses, Reidel, Dordrecht, 1986.
[27] I. Mihalcescu, J.C. Vial, R. Romestain, Phys. Rev. Lett. 80 (1998) 3392.
[28] U. Even, K. Rademann, J. Jortner, N. Manor, R. Reisfeld, Phys. Rev. Lett. 52 (1984) 2164.
[29] J.C. Phillips, Rep. Progress Phys. 59 (1996) 1133.
[30] J. Nelson, S.A. Haque, D.R. Klug, J.R. Durrant, Phys. Rev. B 6320 (2001) (art. no. 205321).
[31] J.A. Anta, J. Nelson, N. Quirke, Phys. Rev. B 65 (2002) (art. no. 125324).
[32] J. Nelson, Phys. Rev. B 59 (1999) 15374.
[33] N. Kopidakis, E.A. Schiff, N.G. Park, J. van de Lagemaat, A.J. Frank, J. Phys. Chem. B 104 (2000) 3930.
[34] J. Bisquert, A. Zaban, Appl. Phys. A-Mater. Sci. Process. 77 (2003) 507.
[35] R.L. Willis, C. Olson, B. O'Regan, T. Lutz, J. Nelson, J.R. Durrant, J. Phys. Chem. B 106 (2002) 7605.
[36] I. Montanari, J. Nelson, J.R. Durrant, J. Phys. Chem. B 106 (2002) 12203.
[37] D. Kuciauskas, M.S. Freund, H.B. Gray, J.R. Winkler, N.S. Lewis, J. Phys. Chem. B 105 (2001) 392.
[38] C.A. Kelly, F. Farzad, D.W. Thompson, J.M. Stipkala, G.J. Meyer, Langmuir 15 (1999) 7047.
[39] I.G. Austin, N.F. Mott, Adv. Phys. 50 (2001) 757.
[40] V.N. Bogomolov, E.K. Kudinov, D.N. Mirlin, Y.A. Firsov, Sov. Phys. Solid State 9 (1968) 1630.
[41] W. Gopel, J.A. Anderson, D. Frankel, M. Jaehnig, K. Phillips, J.A. Schafer, G. Rocker, Surf. Sci. 139 (1984) 333.
[42] W.C. Mackrodt, E.A. Simson, N.M. Harrison, Surf. Sci. 384 (1997) 192.
[43] A.G. Thomas, W.R. Flavell, A.R. Kumarasinghe, A.K. Mallick, D. Tsoutsou, G.C. Smith, R. Stockbauer, S. Patel, M. Gratzel, R. Hengerer, Phys. Rev. B 67 (2003) (art. no. 035110).
[44] F. Cao, G. Oskam, P.C. Searson, J.M. Stipkala, T.A. Heimer, F. Farzad, G.J. Meyer, J. Phys. Chem. 99 (1995) 11974.
[45] A. Henningsson, H. Rensmo, A. Sandell, H. Siegbahn, S. Sodergren, H. Lindstrom, A. Hagfeldt, J. Chem. Phys. 118 (2003) 5607.
[46] J. Muscat, N.M. Harrison, G. Thornton, Phys. Rev. B 59 (1999) 15457.
[47] B. Oregan, M. Gratzel, D. Fitzmaurice, Chem. Phys. Lett. 183 (1991) 89.
[48] R.F. Howe, M. Gratzel, J. Phys. Chem. 89 (1985) 4495.
[49] U. Kolle, J. Moser, M. Gratzel, Inorg. Chem. 24 (1985) 2253.
[50] G. Boschloo, D. Fitzmaurice, J. Phys. Chem. B 103 (1999) 2228.
[51] A.V. Barzykin, M. Tachiya, J. Phys. Chem. B 106 (2002) 4356.
[52] N.W. Duffy, L.M. Peter, R.M.G. Rajapakse, K.G.U. Wijayantha, Electrochem. Commun. 2 (2000) 658.
[53] A.C. Fisher, L.M. Peter, E.A. Ponomarev, A.B. Walker, K.G.U. Wijayantha, J. Phys. Chem. B 104 (2000) 949.
[54] A. Green, J.R. Durrant, private communication, 2003.
[55] C.L. Olson, Ph.D. Thesis, Department of Physics, University of London, 2003.
[56] A.F. Nogueira, I. Montanari, J. Nelson, J.R. Durrant, C. Winder, N.S. Sariciftci, J. Phys. Chem. B 107 (2003) 1567.
[57] J. Nelson, Phys. Rev. B 67 (003) (art. no. 155209).
[58] S. Kambe, S. Nakade, T. Kitamura, Y. Wada, S. Yanagida, J. Phys. Chem. B 106 (2002) 2967.
[59] J.N. Clifford, G. Yahioglu, L.R. Milgrom, J.R. Durrant, Chemical Communications (2002) 1260-1261.
[60] J.N. Clifford, E. Palomares, M.K. Nazeeruddin, M. Gratzel, J. Nelson, J.R. Durrant, J. Am. Chem. Soc. (2003), in press.
[61] E. Palomares, J.N. Clifford, S.A. Haque, T. Lutz, J.R. Durrant, J. Am. Chem. Soc. 125 (2003) 475.
[62] G. Franco, J. Gehring, L.M. Peter, E.A. Ponomarev, I. Uhlendorf, J. Phys. Chem. B 103 (1999) 692.
[63] N.W. Duffy, L.M. Peter, R.M.G. Rajapakse, K.G.U. Wijayantha, J. Phys. Chem. B 104 (2000) 8916.
[64] S.A. Haque, J. Nelson, J.R. Durrant, in: Photovoltaics for the 21st Century, Electrochemical Society, Washington, 2001.
[65] A.N.M. Green, R.E. Chandler, S.A. Haque, J. Nelson, J.R. Durrant, J. Phys. Chem. B (2004), in press.
[66] K. Zhu, E.A. Schiff, N.G. Park, J. van de Lagemaat, A.J. Frank, Appl. Phys. Lett. 80 (2002) 685.
[67] D. Bahnemann, A. Henglein, J. Lilie, L. Spanhel, J. Phys. Chem. 88 (1984) 709.
[68] Y. Liu, A. Hagfeldt, X.R. Xiao, S.E. Lindquist, Solar Energy Mater. Solar Cells 55 (1998) 267.
[69] S.Y. Huang, G. Schlichthorl, A.J. Nozik, M. Gratzel, A.J. Frank, J. Phys. Chem. B 101 (1997) 2576.
[70] S.A. Haque, Ph.D. Thesis, Department of Chemistry, University of London, 2000.
[71] A. Hagfeldt, M. Gratzel, Acc. Chem. Res. 33 (2000) 269.
[72] M.J. Cass, F.L. Qiu, A.B. Walker, A.C. Fisher, L.M. Peter, J. Phys. Chem. B 107 (2003) 113.
[73] K.D. Benkstein, N. Kopidakis, J. van de Lagemaat, A.J. Frank, J. Phys. Chem. B 107 (2003) 7759.
[74] M.N. Jacouris, M. Res. Thesis, Department of Chemistry, Imperial College London, 2003.
[75] J.N. Clifford, E. Palomares, M.K. Nazeeruddin, M. Gratzel, J. Nelson, J.R. Durrant, J. Am. Chem. Soc. (2004), in press.